

International Journal of Modern Physics E
 © World Scientific Publishing Company

Thermal conductivity of hot pionic medium due to pion self-energy for $\pi\sigma$ and $\pi\rho$ loops

Sabyasachi Ghosh

*Instituto de Física Teórica, Universidade Estadual Paulista,
 Rua Dr. Bento Teobaldo Ferraz, 271, 01140-070 Sao Paulo, SP, Brazil
 sabyaphy@gmail.com*

The thermal conductivity of pionic medium has been evaluated with the help of its standard expression from the relaxation time approximation, where inverse of pion relaxation time or pion thermal width has been obtained from the imaginary part of pion self-energy. In the real-time formalism of thermal field theory, the finite temperature calculations of pion self-energy for $\pi\sigma$ and $\pi\rho$ loops have been done. The numerical value of our thermal conductivity increases with temperature very softly, though at particular temperature, our estimation has to consider a large band of phenomenological uncertainty.

Keywords: Thermal Field Theory; Thermal conductivity; Hadronic Matter.

PACS numbers:

1. Introduction

In order to describe the expanding fire ball, produced at RHIC or LHC, the inclusion of dissipative effects in hydrodynamical and transport simulations has attracted remarkable attention in the recent years. Only the shear viscosity of the expanding matter is taken as a relevant dissipative coefficient by most of the communities, doing such kind of simulations. To explain the elliptic flow parameter, v_2 , extracted from data collected at RHIC and LHC, their investigations suggest that the matter is likely to have a very small ratio of shear viscosity to entropy density, η/s . As a next attempt, the inclusion of bulk viscosity coefficient (ζ) in those simulations has been started in a few studies but the effect of thermal conductivity (κ) on those time evolution pictures of expanding matter is largely ignored except the recent Refs,^{1,2} trying to develop a model of the thermal conductivity. This is because the thermal conduction does not take place very well in the system, where net baryon density is approximately zero.³⁻⁵ Most of the hydrodynamical simulations are focused on describing the baryon-free matter, which is expected to be created in the central rapidity region at the RHIC and LHC. However, thermal conductivity definitely demands its attention to describe the expanding fire ball at forward rapidities or at smaller collision energies, such as those at FAIR and in the low-energy runs at RHIC. Probably for same reason, the microscopic calculation of thermal conductivity for

Table 1. Numerical values of thermal conductivity κ of some earlier works in the hadronic temperature domain $T \approx 0.12 - 0.17$ GeV or near the transition temperature.

Earlier works (adopted model or method)	κ (GeV ²)
Ref. ¹⁴ (NJL model)	11.6-7.78
Ref. ¹⁴ (DPQM model)	4.5
Ref. ¹⁰ (Liquid-instanton model)	0.12
Ref. ¹¹ (unitarization method)	0.07-0.1
Ref. ⁵ (CEA method)	0.032-0.049
Ref. ⁵ (RTA method)	0.016-0.02
Ref. ⁴ (BAMPS, $\sigma \approx 43$ mb)	$2.59/\sigma \approx 0.023$
Ref. ⁹ (CEA method)	0.015-0.024
Ref. ³ (RTA method)	0.016-0.024
Ref. ⁸ (CEA method)	0.016-0.024
Ref. ⁷ (unitarization method)	0.007-0.008

the strongly interacting matter is not extensively explored to know its explicit temperature dependence as done rigorously for the other dissipative quantities viz. shear and bulk viscosities. To date, only a few studies have addressed calculation of thermal conductivity of the strongly interacting matter.³⁻¹⁶ Their estimations collectively exhibit a band of predictions as shown in the Table 1.

Here our interest is to calculate the thermal conductivity of pionic medium, which may also appear in between the chemical and kinetic freeze-out temperatures ($T_{ch} \approx 0.17$ GeV to $T_f \approx 0.12$ GeV) at zero baryon chemical potential of the expanding fire ball during its late stage. Though the pionic constituent particles do not carry any baryon number but for the medium with finite pion chemical potential μ_π , where total number of pion remain constant, may have a non-zero value of thermal conductivity.^{3,5} We will make our estimation for $\mu_\pi = 0$, which will help to compare with other relevant results.

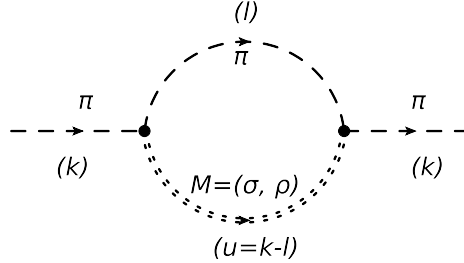
2. Formalism

Let us start from the standard expression of thermal conductivity for pionic medium in the relaxation time approximation (RTA)³ :

$$\kappa = \frac{\beta^2 I_\pi}{6\pi^2} \int_0^\infty \frac{d\vec{k} \vec{k}^4}{\omega_k^{\pi 2} \Gamma_\pi} (\omega_k^\pi - h_\pi)^2 n_k(\omega_k^\pi) \{1 + n_k(\omega_k^\pi)\}, \quad (1)$$

where $n_k(\omega_k^\pi) = 1/\{e^{\beta\omega_k^\pi} - 1\}$ is the Bose-Einstein (BE) distribution function of pion with $\omega_k^\pi = (\vec{k}^2 + m_\pi^2)^{1/2}$, and $\Gamma_\pi (= 1/\tau_\pi, \tau_\pi$ is pion relaxation time) is the thermal width of π mesons in the medium. Here $I_\pi = 3$ is pion isospin factor and h_π is the exact heat function per particle for the pionic medium, which can be estimated from the ideal gas expression,

$$h_\pi = (e_\pi + p_\pi)/\rho_\pi = T s_\pi/\rho_\pi, \quad (2)$$


 Fig. 1. Pion self-energy diagram for $\pi\sigma$ and $\pi\rho$ loops.

where

$$s_\pi = I_\pi \beta \int \frac{d^3 \vec{k}}{(2\pi)^3} \left(\omega_k^\pi + \frac{\vec{k}^2}{3\omega_k^\pi} \right) n_k(\omega_k^\pi) \quad (3)$$

and

$$\rho_\pi = I_\pi \int \frac{d^3 \vec{k}}{(2\pi)^3} n_k(\omega_k^\pi) \quad (4)$$

are entropy density and number density respectively of the pionic medium at temperature $T = 1/\beta$.

Now, the thermal width, Γ_π for pion can be determined from the imaginary part of its one-loop self-energy^{17–20} at finite temperature, by the relation:

$$\begin{aligned} \Gamma_\pi(\vec{k}, T) &= \sum_M \Gamma_{\pi(\pi M)}(\vec{k}, T) \\ &= - \sum_M \text{Im} \Pi_{\pi(\pi M)}^R(k_0 = \omega_k^\pi, \vec{k}, T) / m_\pi. \end{aligned} \quad (5)$$

In the above equation, $\Pi_{\pi(\pi M)}^R$ is the retarded component of pion self-energy for πM loops, where M stands for σ and ρ resonances. Feynman diagram of pion self energy for πM loops is shown in the Fig. (1), where k is the momentum of external π line while l and $u = k - l$ are momenta of internal π and M lines respectively.

Following the effective hadronic model as adopted in earlier Refs,^{17, 20, 21} the σ and ρ resonances in $\pi\pi$ scattering have traditionally been introduced by using the effective Lagrangian densities for $\pi\pi\sigma$ and $\pi\pi\rho$ interactions:

$$\mathcal{L} = g_\rho \vec{\rho}_\mu \cdot \vec{\pi} \times \partial^\mu \vec{\pi} - \frac{g_\sigma}{2} m_\sigma \vec{\pi} \cdot \vec{\pi} \sigma, \quad (6)$$

where the coupling constants ($g_\sigma = 5.82$ and $g_\rho = 6$) are fixed from their experimental decay widths of σ and ρ mesons in their $\pi\pi$ channels.¹⁷ The negative sign in the second term for $\sigma\pi\pi$ coupling is important to determine the relative phase.²² With the help of the above Lagrangian densities (6), pion self-energy for πM loops (shown in Fig. 1) with $M = \sigma$ and ρ can be derived in the real-time formalism of thermal field theory.¹⁷ As the pion pole ($k_0 = \omega_k^\pi, \vec{k}$) is situated in the Landau cut

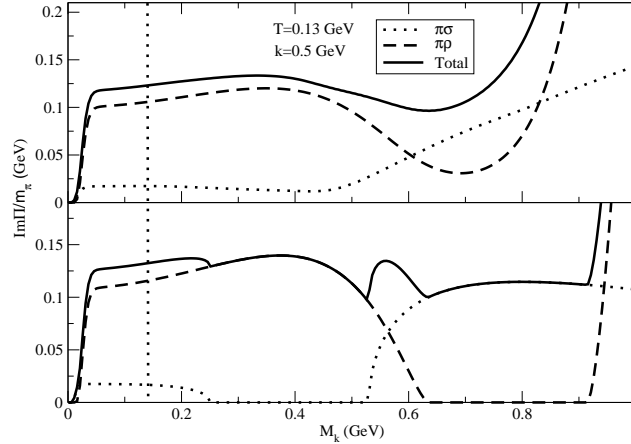
4 *Sabyasachi Ghosh*


Fig. 2. Invariant mass distribution function, $\Gamma_{\pi(\pi M)}(M_k) = \text{Im}\Pi_{\pi(\pi M)}^R(M_k)/m_\pi$ for $\pi\sigma$ (dotted line), $\pi\rho$ (dashed line) loops and their total (solid line) at fixed values of \vec{k} and T . Upper and lower panels consist the results with and without folding effect respectively.

of the self-energy function, $\Pi_{\pi(\pi M)}^R(k_0, \vec{k})$ so the corresponding thermal width can simply be expressed as^{17–20}

$$\begin{aligned} \Gamma_{\pi(\pi M)}(\vec{k}, T) &= \text{Im}\Pi_{\pi(\pi M)}^R(k_0 = \omega_k^\pi, \vec{k}, T)/m_\pi \\ &= \frac{1}{m_\pi} \left[\int \frac{d^3\vec{l}}{(2\pi)^3} L(l_0 = -\omega_l^\pi, \vec{l}, k) \{n_l(\omega_l^\pi) \right. \\ &\quad \left. - n_u(\omega_u^M)\} \delta(k_0 + \omega_l^\pi - \omega_u^M) \right]_{k_0 = \omega_k^\pi}, \end{aligned} \quad (7)$$

where n_l and n_u are BE distribution functions of π and M mesons respectively. Using the effective Lagrangian densities (6), one can obtain the vertex factors:

$$\begin{aligned} L(k, l) &= -\frac{g_\sigma^2 m_\sigma^2}{4}, \text{ for } M = \sigma, \\ &= -\frac{g_\rho^2}{m_\rho^2} [k^2 (k^2 - m_\rho^2) + l^2 (l^2 - m_\rho^2) - 2\{(k \cdot l) m_\rho^2 + k^2 l^2\}], \text{ for } M = \rho. \end{aligned} \quad (8)$$

A hadronic form factor $F(\vec{l}) = \Lambda^2/(\vec{l}^2 + \Lambda^2)$ with $\Lambda = 1$ GeV has been multiplied with each of the effective coupling constants, g_σ and g_ρ to consider finite size effect of hadronic vertices.

3. Results and Discussion

Let us start our discussion of numerical results from the pion thermal widths, which inversely control the numerical strength of thermal conductivity of pionic medium.

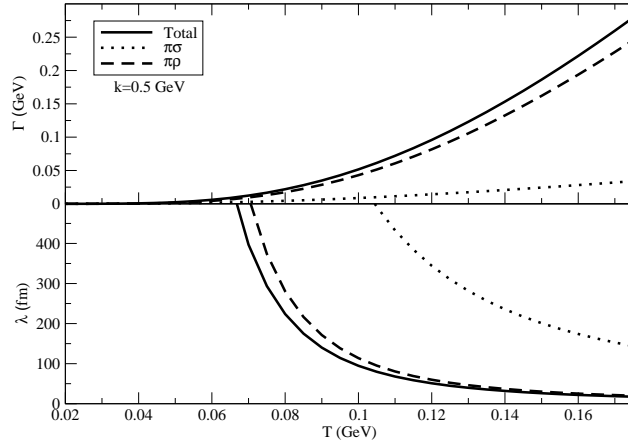


Fig. 3. At fixed pion momentum ($\vec{k} = 0.5$ GeV), the temperature dependence of $\Gamma_{\pi(\pi\sigma)}$ (dotted line), $\Gamma_{\pi(\pi\rho)}$ (dashed line) and their total (solid line) are shown in the upper panel whereas lower panel demonstrates the corresponding mean free path contributions of two individual loops and their total.

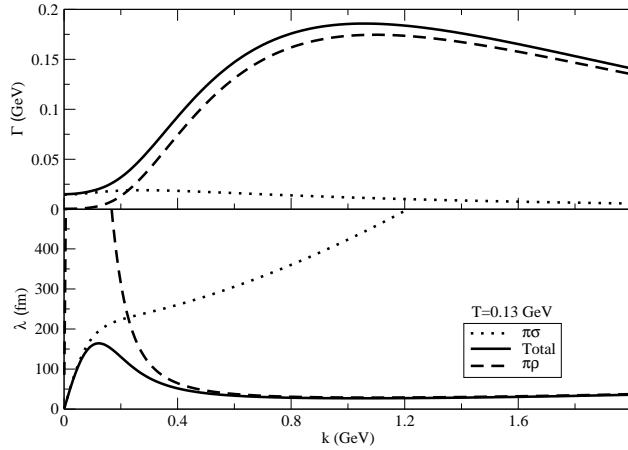


Fig. 4. Similar to Fig. (3), for a fixed value of T against \vec{k} -axis.

In Fig. (2), the off-mass shell behavior of $\Gamma_{\pi(\pi M)}(M_k, \vec{k}, T)$ is plotted against the invariant mass axis M_k before going to analyze the on-shell function $\Gamma_{\pi(\pi M)}(M_k = m_\pi, \vec{k}, T)$. The numerical values of $\Gamma_{\pi(\pi M)}(M_k, \vec{k}, T)$ can be generated if we replace $k_0 = \{\vec{k}^2 + m_\pi^2\}^{1/2}$ by $k_0 = \{\vec{k}^2 + M_k^2\}^{1/2}$ in Eq. (7) for fixed values of pion momentum ($\vec{k} = 0.5$ GeV) and temperature of the medium ($T = 0.13$ GeV). In the lower panel of Fig. (2), the dotted line is representing the Landau and unitary cut contributions for $\pi\sigma$ loop in the regions ($M_k = 0$ to $m_\sigma - m_\pi = 0.25$ GeV)

and ($M_k = m_\sigma + m_\pi = 0.53$ GeV to ∞) respectively. Similarly, the dashed line is displaying the corresponding Landau and unitary cut contributions for $\pi\rho$ loop in the regions ($M_k = 0$ to $m_\rho - m_\pi = 0.63$ GeV) and ($M_k = m_\rho + m_\pi = 0.91$ GeV to ∞) respectively. Owing to the broad spectral width of σ and ρ resonances, we have folded the pion thermal width $\Gamma_{\pi(\pi M)}$ by the vacuum spectral functions of those resonances as we have done in our previous work¹⁷ to calculate shear viscosity. The multi-peak structure of total $\Gamma_{\pi(\pi M)}(M_k)$ (solid line in the lower panel) is polished to a smooth curve (solid line in the upper panel) after introducing the folding effect. This is because the region of branch cuts are generally overlapped to each other during the folding operation, which is reflected by the dotted and dashed lines for $\pi\sigma$ and $\pi\rho$ loops in the upper panel of Fig. (2). The on-shell contribution of the pion thermal width (i.e. $\Gamma_{\pi(\pi M)}(M_k = m_\pi)$) has been indicated by the straight dotted line in the Fig. (2), where we see that the contribution of $\pi\rho$ loop dominates over the $\pi\sigma$ loop and its total value becomes little smaller due to folding effect.

This on-shell contribution from the Landau cut is associated with the forward and reverse scattering processes.²³ In the forward process, the propagating π^+ may disappear by absorbing a thermalized π^- from the medium to create a thermalized ρ^0 or σ . Whereas in the reverse process, the π^+ may appear by absorbing a thermalized ρ^0 or σ from the medium as well as by emitting a thermalized π^- .

In upper panel of Fig. (3), the on-shell contribution of $\pi\sigma$ (dotted line), $\pi\rho$ (dashed line) loops and total (solid line) thermal width for pion are plotted against temperature axis. Contributions of both loops are monotonically increasing functions but $\pi\rho$ takes leading part in the total contribution. The corresponding results for mean free path, defined by $\lambda_{\pi(\pi M)} = \vec{k}/(\omega_k^\pi \Gamma_{\pi(\pi M)})$, are shown in the lower panel of Fig. (3). Being inverse of thermal width, the mean free paths become decreasing functions of T .

The momentum distribution for different components of thermal widths and mean free paths are presented in the upper and lower panels of Fig. (4). Upper panel shows that the pion thermal width for $\pi\sigma$ (dotted line) and $\pi\rho$ (dashed line) loops become significant in the low and high momentum regions respectively. The corresponding mean free paths in the lower panel of the figure expose this complementary feature of two resonances in more prominent way. Here we notice that mean free path contribution from $\pi\sigma$ loop is tending to diverge after $\vec{k} \approx 0.1$ GeV while divergent nature for $\pi\rho$ loop contribution is starting below the $\vec{k} \approx 0.2$ GeV. A phenomenological lesson from this fact is that the low momentum pion will get the relevant dissipation by scattering with σ resonance whereas the dissipation of high momentum pion will be coming from the $\pi\rho$ scattering in the medium.

Using the thermal width $\Gamma_{\pi(\pi M)}(\vec{k}, T)$ in Eq. (1), one can estimate the thermal conductivity, which possesses the temperature dependence from not only the thermal width but also the Bose-enhanced phase space factor of pions. The contributions of $\pi\sigma$ (dotted line), $\pi\rho$ (dashed line) loops and their total (solid line) in the thermal conductivity are presented as functions of temperature in the Fig. (5),

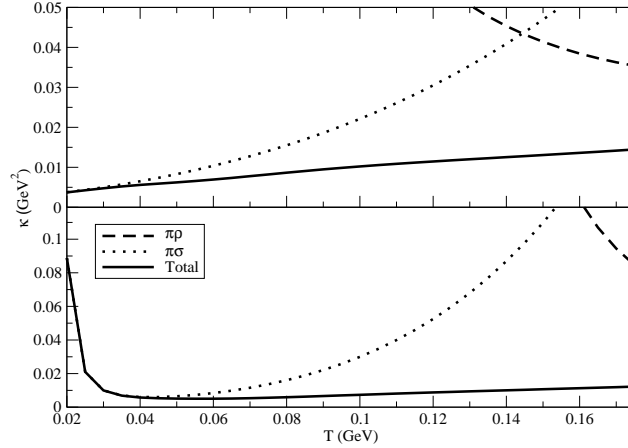


Fig. 5. The contributions of $\pi\sigma$ (dotted line), $\pi\rho$ (dashed line) loops and their total in the thermal conductivity κ are plotted against T axis. The upper and lower panels of this figure and latter Figs. (6) and (7) are allotted for demonstrating with and without folding results respectively.

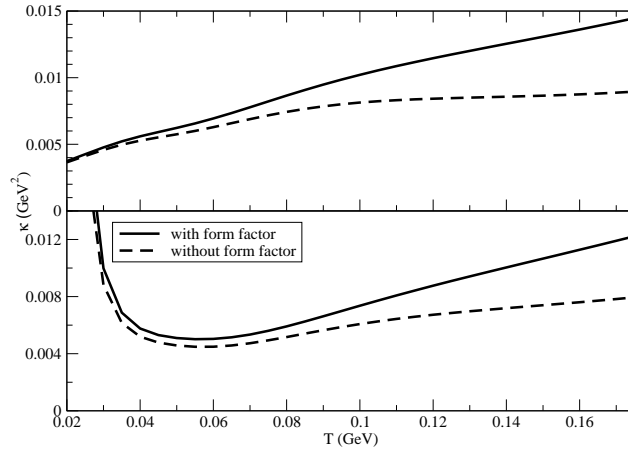


Fig. 6. T dependence of κ without (dashed line) and with (solid line) form factor.

where the upper and lower panels show the results with and without folding respectively. The $\kappa_\pi(T)$ due to $\pi\rho$ loop appears as a decreasing function and diverges in low temperature region, where $\pi\sigma$ loop has a finite contributions. Because of this compensating nature of two loops, $\kappa_\pi(T)$ for the mesonic system is revealed as non-divergent well behaved function in the entire temperature domain. Though the total thermal conductivity without folding effect (lower panel) is exhibiting a divergent nature at very low temperatures ($T < 0.020$ GeV) but this divergence is

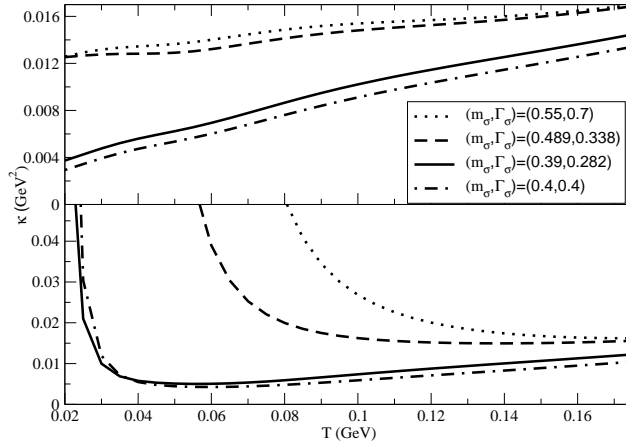


Fig. 7. Total $\kappa(T)$ for different set of mass m_σ (GeV) and width Γ_σ (GeV) of σ meson, taken from Refs.^{24, 25, 27, 28} by following the previous Ref.¹⁷

cured completely after incorporating the folding effect (upper panel).

Similar to folding effect, our results can also be influenced by cut-off parameter Λ of the hadronic form factor, which is taken in the $\pi\pi M$ vertex. The results without form factor (dashed line) yield the minimum values of κ vs T curve, whereas results with form factor (solid line) exhibit the enhanced values of κ as shown in Fig. (6). Owing to this fact, the thermal conductivity in our effective hadronic model may vary within a band; e.g. $\kappa = 0.0086 - 0.013 \text{ GeV}^2$ at $T = 0.15 \text{ GeV}$.

Besides this, our results may suffer from phenomenological uncertainty for fixing the parameters of σ resonance as discussed in our earlier work on shear viscosity.¹⁷ Longstanding controversies about the properties of σ resonance seem to be settling to a consensus²⁹ as the band of its mass-width values have been shortened from $(m_\sigma = 0.4 - 1.2 \text{ GeV}, \Gamma_\sigma = 0.6 - 1 \text{ GeV})$ ³⁰ to $(m_\sigma = 0.4 - 0.55 \text{ GeV}, \Gamma_\sigma = 0.4 - 0.7 \text{ GeV})$.²⁸ Using the minimum (dash-dotted line) and maximum (dotted) values of $(m_\sigma, \Gamma_\sigma)$ from latest PDG,²⁸ the band of κ without (lower panel) and with (upper panel) folding effect are shown in Fig. 7. The results of κ , for the mass-width parameters taken from BES^{25, 26} (solid line) and E791²⁷ (dashed line) experiments, are also included in the Fig. (7). Among them, the set of $(m_\sigma, \Gamma_\sigma)$ from BES experiment is arbitrarily chosen to generate all the previous results, shown in Fig. (2) to (6). The list of effective coupling (g_σ) is provided in the Table of Ref.¹⁷ From the upper panel of Fig. (7), κ at $T = 0.15 \text{ GeV}$ may vary from 0.012 GeV^2 to 0.016 GeV^2 . Hence, adding the uncertainty of σ meson parameters with the form factor effect, we get $\kappa(T = 0.15 \text{ GeV}) = 0.0086 - 0.016 \text{ GeV}^2$, which is exhibiting quite large band of prediction of thermal conductivity from the effective hadronic model. From the Table (1), one can notice that the numerical values of κ of earlier Refs.^{3-5, 7-11} are within the band of uncertainty, contained in our results.

4. Summary

In Summary, an estimation of thermal conductivity for pionic medium has been done with the help of the effective hadronic model. We have started with the standard expression of thermal conductivity in RTA approach, where inverse of pion relaxation time (τ_π) or pion thermal width Γ_π has been evaluated from the imaginary part of pion self-energy. Keeping in mind about the appearance of σ , ρ resonances in the $\pi\pi$ scattering cross section, we have evaluated pion self-energy for $\pi\sigma$ and $\pi\rho$ loops in the real-time formalism of thermal field theory. We get a non-monotonic momentum distribution of pion thermal width, which has to be integrated out by the Bose-enhanced phase factor during estimation of thermal conductivity. Our estimation has a large band of uncertainty because of the various phenomenological parameters such as mass-width parameter of sigma meson, hadronic form factor etc. Some^{3-5, 7-11} of the earlier estimation of thermal conductivity for strongly interacting matter in hadronic temperature domain are within our band of estimation.

Acknowledgment : Work is financed by Fundação de Amparo à Pesquisa do Estado de São Paulo - FAPESP, Grant Nos. 2012/16766-0. I am very grateful to Prof. Gastao Krein for his academic and non-academic support during my postdoctoral period in Brazil.

References

1. J. I. Kapusta and J. M. Torres-Rincon, Phys. Rev. **C 86**, 054911 (2012).
2. G. Denicol, H. Niemi, I. Bouras, E. Molnar, Z. Xu, D. H. Rischke, C. Greiner, Phys. Rev. **D 89**, 074005 (2014).
3. S. Gavin, Nucl. Phys. A **435**, 826 (1985).
4. M. Greif, F. Reining, I. Bouras, G. S. Denicol, Z. Xu, and C. Greiner, Phys. Rev. **E 87**, 033019 (2013).
5. S. Mitra, S. Sarkar, Phys. Rev. **D 89**, 054013 (2014).
6. S. Mitra, U. Gangopadhyaya, S. Sarkar, Phys. Rev. **D 91**, 094012 (2015).
7. D. Fernandez-Fraile and A. Gomez Nicola, Eur. Phys. J. **C 62**, 37 (2009).
8. M. Prakash, M. Prakash, R. Venugopalan, and G. Welke, Phys. Rep. **227**, 321 (1993).
9. D. Davesne, Phys. Rev. **C 53**, 3069 (1996).
10. S. Nam, Mod. Phys. Lett. **A 30**, 1550054 (2015).
11. A. Dobado, F. J. Llanes-Estrada, J. M. Torres Rincon arXiv:hep-ph/0702130.
12. S. Mattiello, arXiv:1210.1038 [hep-ph].
13. M. Iwasaki and T. Fukutome, J. Phys. G **36**, 115012 (2009).
14. R. Marty, E. Bratkovskaya, W. Cassing, Jr. Aichelin and H. Berrehrah, Phys. Rev. **C 88**, 045204 (2013).
15. I. A. Shovkovy and P. J. Ellis, Phys. Rev. **C 66**, 015802 (2002).
16. M. Braby, J. Chao and T. Schfer, Phys. Rev. **C 81**, 045205 (2010).
17. S. Ghosh, G. Krein, S. Sarkar, Phys. Rev. **C 89** (2014) 045201.
18. S. Ghosh, Phys. Rev. **C 90** (2014) 025202.
19. S. Ghosh, Int. J. Mod. Phys. **A 29** (2014) 1450054.
20. S. Ghosh, J. Phys. G **41** (2014) 095102.
21. S. Mitra, S. Ghosh, and S. Sarkar Phys. Rev. **C 85**, 064917 (2012).
22. M. Harada, F. Sannino, J. Schechter, Phys. Rev. **D 54**, 3 (1996).
23. H.A. Weldon, Phys. Rev. **D 28**, 2007 (1983).

10 *Sabyasachi Ghosh*

24. M.C. Menchaca-Maciel and J.R. Morones-Ibarra, Indian J. Phys. **87**, 385 (2013).
25. W. Huo, X. Zhang, and T. Huang Phys. Rev. D **65**, 097505 (2002).
26. S. Ishida, M.Y. Ishida, H. Takahashi, T. Ishida, K. Takamatsu, and T. Tsuru, Prog. Theor. Phys. **95**, 745 (1996).
27. E. M. Aitala *et al.* (Fermilab E791 Collaboration) Phys. Rev. Lett. **86**, 770 (2001)
28. J. Beringer et al. (*Particle Data Group*) Phys. Rev. D **86**, 010001 (2012).
29. J. R. Peláez, POS (Confinement X) 019 (2012), arXiv:1301.4431v1.
30. K Nakamura *et al.* (*Particle Data Group*) J. Phys. G **37**, 075021 (2010)